Late-Holocene counterpoint deposition in the Lower Rhine River

LISA BOTERMAN (iD), JASPER CANDEL, BART MAKASKE and JAKOB WALLINGA (iD)
Soil Geography and Landscape Group, Wageningen University and Research, Droevendaalsesteeg 3, Wageningen 6700 AA, The Netherlands (E-mail: jasper.candel@wur.nl)

ABSTRACT

Channel deposits from meandering rivers have proven to be far more complex than the well-known lithofacies model consisting of coarse-grained channel, gravelly channel-lag and fine-grained overbank deposits. Sharp bends in rivers are subject to different hydraulic processes than bends with lower curvatures, enabling erosion of inner banks and deposition of fine-grained sediments in the outer bend, resulting in downstream migration of river bends. This phenomenon is known as counterpoint deposition, forming counterpoint bars. This research investigates whether scroll bars associated with a sharp bend in the Lower Rhine River, The Netherlands, are such a counterpoint-bar deposit. A counterpoint bar is expected based on: (i) the surface morphology of the scroll bar; (ii) the confinement of the river course by an ice-pushed ridge resulting in a sharp bend; and (iii) the archaeological context of successive Roman settlements atop the ice-pushed ridge, potentially moving downstream with the migrating river bend. This hypothesis is tested through detailed borehole descriptions combined with optically stimulated luminescence dating, the latter being a novel approach to identifying counterpoint deposits. The deposits consist of clays and sandy clays with fine sand laminations, and sporadic larger sand bodies. Further upstream these deposits grade into channel deposits dominated by coarser sands with gravels. These lithologies are explained using earlier proposed mechanisms for counterpoint formation; substrata match those described in previously studied counterpoint deposits and their point bar counterparts. Optically stimulated luminescence dates indicate that the Lower Rhine River bend migrated downstream, confirming counterpoint deposition. A migration rate of 1.93 m/year was established through weighted linear regression. This study demonstrates the potential of optically stimulated luminescence dating to investigate counterpoint bar presence. The identified counterpoint bars and associated bend migration provide insight into meandering river dynamics that is crucial for river management and in aiding river restoration and rewilding initiatives.

Keywords Counterpoint deposition, downstream migration, fluvial sedimentology, meandering, point bar.

INTRODUCTION

Understanding river dynamics, channel morphology and fluvial processes is essential in a country such as The Netherlands, where proximity to water bodies has made river and stream management an inherent part of society. The topographic and subsurface characteristics of channel belts in the Rhine-Meuse alluvial plain largely define landscape identity (Berendsen, 1982) and have an

extensive effect on spatial planning (Winkels et al., 2020). Meandering channel deposits, however, have proven to be far more complex than the well-known lithofacies model consisting of coarse-grained channel, gravelly channel-lag and fine-grained overbank deposits (Allen, 1965). It is becoming widely recognized that fine-grained in-channel deposits, instead of only overbank deposits, also contribute significantly to the fine-grained consistency of floodplains (Nanson, 1980; Page & Nanson, 1982; Makaske & Weerts, 2005; Smith et al., 2009, 2011; Candel et al., 2020; Sylvester et al., 2021; Winkels et al., 2022). One example of such deposits are counterpoint deposits that form counterpoint bars. This study focusses on the recognition of these deposits in an outer bend of the Lower Rhine River.

Counterpoint bars describe the fine-grained, silty or clayey counterparts to point bars that form at the downstream tail of a point bar and in the concave (outer) bank of the river (Page & Nanson, 1982; Nanson & Croke, 1992; Fig. 1). These deposits can form in sharply curved meander bends (Page & Nanson, 1982; Nanson & Croke, 1992; Smith et al., 2009), in bends where the outer banks are erosion-resistant, for example in confined meander belts with limited floodplain width (Nicoll & Hickin, 2010), or where lateral migration of the channel is prevented by cohesive mud-filled residual channels (Smith et al., 2009; Candel et al., 2020). Bend sharpness can be defined as the ratio between curve radius (R_{curv}) and channel width (w) (Leeder & Bridges, 1975), with sharp bends commonly being defined as $\frac{R_{curv}}{w} < 2.0$ (Nicoll & Hickin, 2010; Candel et al., 2020). In the context

of erosion-resistant outer banks, counterpoint deposits can form at impingement angles as low as 10 to 40° (Smith et al., 2011). Such meander bends often experience flow separation in the outer bend due to complex shear stresses and pressure gradients (Nanson, 1980; Blanckaert, 2011), causing reduced flow velocity and enabling deposition of fine sediment in the outer bend. Scour-holes are also common features forming in sharp bends (Vermeulen et al., 2014). Conversely, in a more typical smooth meander ($\frac{R_{curv}}{w}$ in the range of 2.0 to 3.0; Leopold & Wolman, 1966), sediment in the outer bend is eroded (Makaske & Weerts, 2005; Smith et al., 2009, 2011). Counterpoint bars differ noticeably from point bars in their lithology, consisting largely of silts and clays, often with a relatively high organic matter content (Nanson & Croke, 1992; Smith et al., 2009). A gradational boundary between a point bar and a counterpoint bar forms around an inflection point across the transition from the convex curvature of a point bar to concave curvature of a counterpoint bar. These curvatures are expressed in the surface morphology as scroll bars. The term scroll bars is used here to describe any fluvial morphology consisting of curved ridges, irrespective of point bar or counterpoint bar origin. Counterpoint-bar deposits are further distinguishable from point-bar deposits in their (concave) surface scroll bar morphology that arc in the upstream direction, compared to (convex) point bar scroll patterns which arc in a downriver direction (Smith et al., 2009). Accretion of sediment in the outer bend of the river results in downstream migration of the meander bend, as opposed to lateral
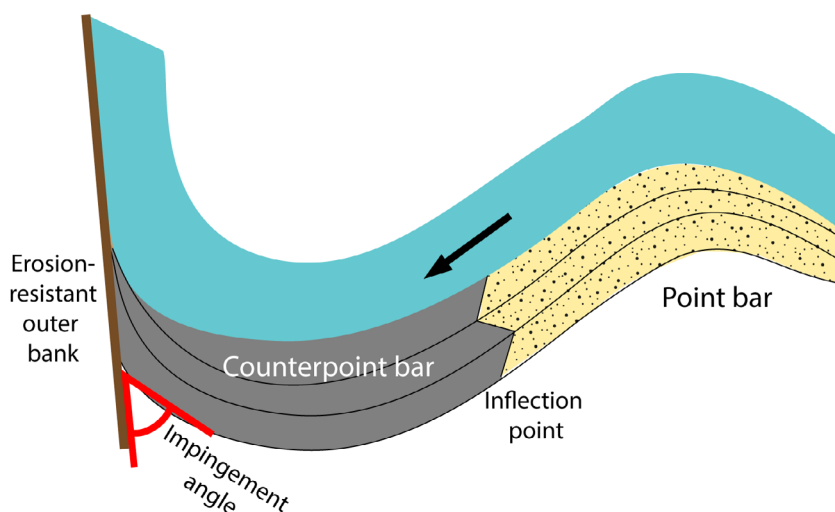

Fig. 1. Schematic figure of a point bar – counterpoint bar transition.

migration often associated with point bar formation.

Counterpoint deposition is a rarely-recognized phenomenon that receives little attention, even in low-gradient environments that are in general favourable for the formation of such deposits (Makaske & Weerts, 2005; Smith *et al.*, 2011). Within the Lower Rhine River a few examples exist of their potential occurrence, although these are limited to smaller channel belts and tributaries. Here, Makaske & Weerts (2005) identified 5 to 6 m thick successions of potential counterpoint deposits along the margins of the Hennisdijk channel belt, an abandoned Rhine distributary dating between 3.9 ka and 3.1 ka. Candel *et al.* (2020) identified counterpoint deposits in a small tributary of the Meuse, the Dommel River, along valley margins and upstream of concave banks dating between 8.5 ka and 2.5 ka. Fine-grained concave accretion deposits have also been identified by Winkels *et al.* (2022) in the Stuivenberg channel belt, a Rhine distributary which was active between 4.3 ka and 3.5 ka. Given the extent of waterways and channel belts within The Netherlands, there is distinct potential for fine-grained counterpoint deposits going unrecognized, which may have consequences for groundwater flow modelling, piping susceptibility (Winkels *et al.*, 2020) and riverbank strength (Candel *et al.*, 2020; Carranza *et al.*, 2022). Downstream, rather than lateral, migration taking place in sharp or restricted river bends could have implications for the planning of river and stream restoration projects, in which groynes and bank protection are being removed (Carranza *et al.*, 2022), and for spatial planning in general. Recirculation and stagnation of flow near the outer bank in sharp bends enable sediment deposition and plant growth (Schnauder & Sukhodolov, 2012), thereby creating habitat, shelter and spawning zones for aquatic species (Schwartz & Herricks, 2005). The potential migration dynamics and ecological functions of these river bends are often ignored in spatial planning and stream restoration practices. It is therefore very relevant that processes associated with counterpoint deposition are accounted for in our co-existence with, and management of, rivers.

Conditions for potential counterpoint bar formation are met at a sharp bend in the Waal River – currently the largest distributary of the Rhine in The Netherlands (Fig. 2A) – flanking the Ooijpolder near Nijmegen. At this location, the topography of an ice-pushed ridge (Fig. 2B), formed when ice sheets last covered (much of)

The Netherlands during Marine Isotope Stage 6 (MIS 6, *ca* 180 to 130 ka), prevents erosion of the outer bank and thus lateral migration. Multiple palaeogeographical reconstructions for the evolution of this meander bend exist, all of which include some manner of meander bend migration by point bar formation in an upstream (south-eastern) direction at the foot of the ice-pushed ridge, followed by cut-off of this bend around Late-Holocene times (Berendsen & Stouthamer, 2000; Cohen *et al.*, 2012; Willemse, 2019). However, this interpretation does not necessarily match the surface scroll bar morphology and is unable to satisfactorily clarify the westward (downstream) succession of multiple Roman fortifications atop the ice-pushed ridge (Fig. 3). Such fortifications were typically built as close as possible to a river (Willems, 1986; Verhagen *et al.*, 2017), and therefore their downstream succession could potentially be associated with river migration. Given also the sharpness of the river bend in question resulting from high impingement angles against the ice-pushed ridge – consisting of material that is topographically and thus physically difficult to erode – it is possible that the resulting flow dynamics enabled counterpoint deposition and downstream instead of lateral migration of the meander bend. This raises the question of whether previously accepted palaeogeographical interpretations of the associated deposits are correct, or whether these deposits are instead counterpoint deposits, which might better fit the geomorphological and archaeological context.

In this research, it was hypothesized that instead of a meander cut-off of the Late-Holocene-aged river bend in the Ooijpolder having occurred, downstream migration of this meander bend to the north-west along the ice-pushed ridge took place, resulting in counterpoint deposition. This was tested through: (i) creating lithological borehole descriptions to determine the extent of fine-grained sediments present in the study area and their resemblance to previously identified counterpoint deposits; and (ii) gathering chronological evidence by optically stimulated luminescence (OSL) dating for the time of deposition of sediments in a transect perpendicular to the surface scroll bar morphology. Based on the results, the depositional mechanisms responsible for the deposits in question are discussed, as well as the implications of the findings for recognizing such features in other river systems.
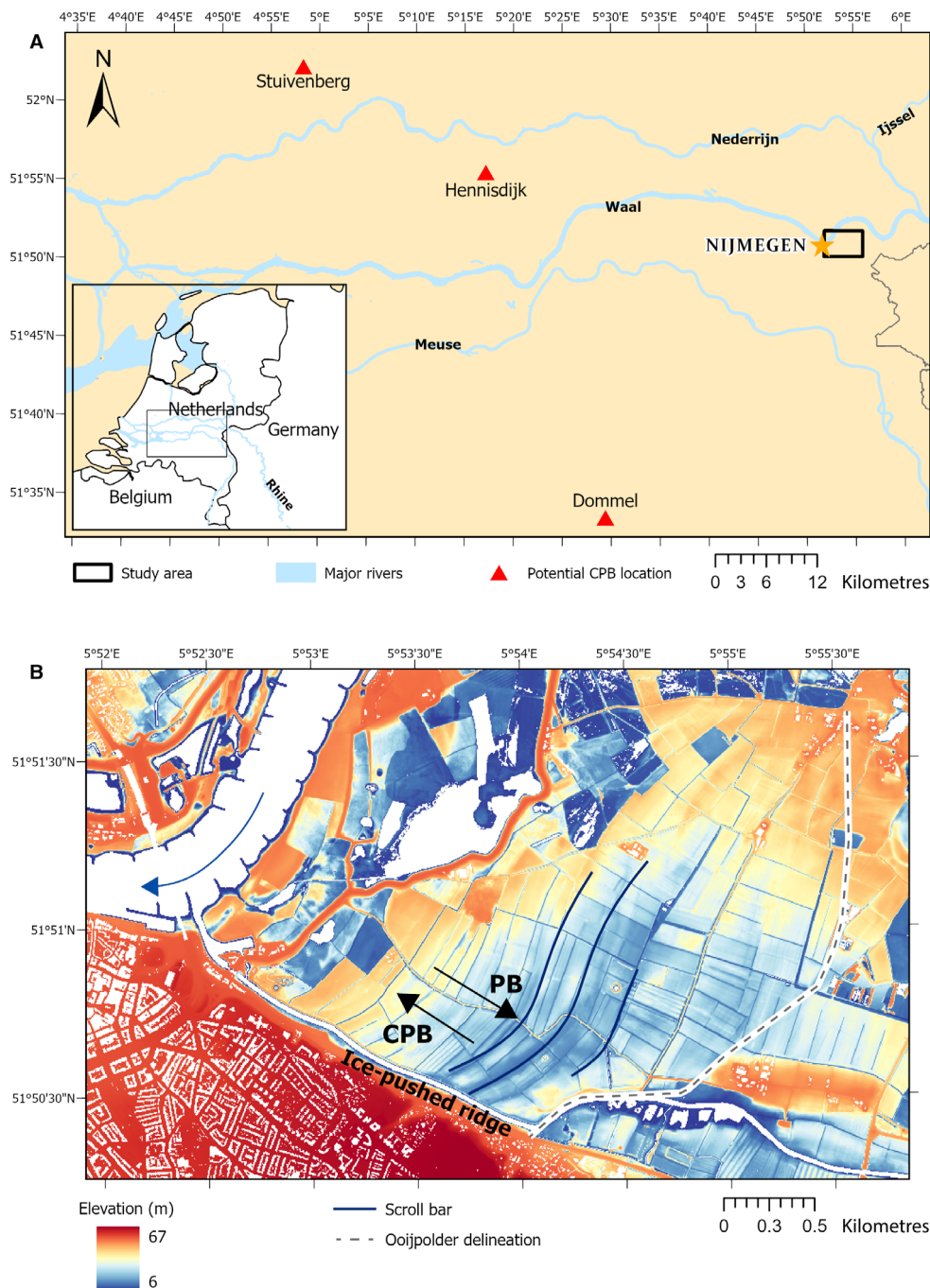
Fig. 2. Maps showing: (A) major rivers of the Rhine-Meuse delta, with locations of potential counterpoint bars (CPB) and the study area (outlined); (B) digital elevation map (Algemeen Hoogtebestand Nederland 3, 0.5 m × 0.5 m; https://www.ahn.nl/) of the study area – outlined in (A), showing the Ooijpolder to the north-east of the ice-pushed ridge (labelled) and south-east of the sharp bend in the Waal River. Sediment accretion direction of the river bend for point bar (PB) and counterpoint bar (CPB) depositional scenarios are shown by black arrows. The blue arrow indicates the direction of flow of the Waal.

STUDY AREA

The Waal River is a sand-bed distributary of the Lower Rhine River (Fig. 2A). The average discharge of the Rhine before bifurcating into the Nederrijn and the Waal is 2300 m³/s (Middelkoop & Haselen, 1999), with the Waal receiving two-thirds of this discharge. The Waal

currently has a depth of around 3 m and is 300 to 400 m wide during average flow conditions (Hobo *et al.*, 2014). Presently, the river is bounded by dykes, the construction of which was completed around 1350 CE (Hobo *et al.*, 2014). Prior to this, the Waal was a freely meandering river (Middelkoop & Haselen, 1999; Hobo *et al.*, 2014; Willemse, 2019) which came into existence around 2000 BP (Stouthamer & Berendsen, 2001). At Nijmegen, south of the Waal River, remnants of an ice-pushed ridge remain (Fig. 2B), which formed during MIS 6 from pre-glacial fluvial sediments (Berendsen & Stouthamer, 2002).

The study area is located in the Ooijpolder – to the south-east of the Waal River and north-east of the ice-pushed ridge (Fig. 2B), encompassing a scroll bar complex formed by a Late-Holocene-aged meander bend of the Waal River (Cohen *et al.*, 2012). This scroll bar complex is clearly visible in the 0.5×0.5 m resolution digital elevation model (DEM) of the study area (Actueel Hoogtebestand Nederland v3; https://www.ahn.nl/; Fig. 2B) upstream of the present channel location. Based on the angles at which these scroll bars meet the ice-pushed ridge, impingement angles of the palaeochannel are estimated to be between 45° and 70°, indicating that the river bend was relatively sharp in the context of counterpoint deposition, as defined by Smith *et al.* (2011). The east of the study area is bound by Late-Pleistocene aged sediments (Cohen & Stouthamer, 2012) and *in situ* Roman-aged archaeological finds (Thijssen & Wildenberg, 2005).

Previous palaeogeographical reconstructions

Multiple palaeogeographical interpretations of the development of the study area during Roman times (12 BCE to 450 CE) exist. Cohen *et al.* (2012) dated the meander system within the Ooijpolder, and the (presumed) associated palaeochannel to have had its channel infilling between 2500 cal. years BP and 1800 cal. years BP, based on a combination of one radiocarbon (^{14}C) date and archaeological and historical evidence (Willems, 1986; Cohen *et al.*, 2012). Willems (1986) suggested that the Roman-aged Waal flowed in approximately the same location as in the present, following a short period (a few centuries) of activity within the Ooijpolder before Roman times. Archaeological and geomorphological studies commissioned by the Dutch government and the municipality of Nijmegen (e.g.

Willemse, 2019; Heunks & van de Geer, 2021), also conclude that point-bar formation and subsequent meander bend cut-off should have taken place during Roman times in order to explain the scroll-bar morphology.

Archaeological context

An overview of Roman settlements and military camps occupied from 19 BCE to the 5th century CE is shown in Fig. 3. Notable about these settlements is that their occupation was never continuous, but rather a series of military camps and civilian settlements were built over, and occupied for, a relatively short period of time. Initial Roman occupation was centred at the Hunerberg and Kops Plateau (Driessen, 2007; Van der Heijden, 2016), while final stages of settlement during the fall of the *limes* (270 CE) and the Roman Empire (450 CE) were located primarily around Ulpia Noviomagus and the present day Valkhof (Willems, 1990). The lack of continuous occupation of these Roman settlements could suggest that external factors, such as migration of the river, were responsible for the Roman's frequent relocation within Nijmegen. Evidence for shipping networks throughout their occupation can be found in their overcoming logistical challenges of feeding their legions (Van der Heijden, 2016), the transition of wooden to (imported) stone infrastructure from 88/89 CE (Driessen, 2007), and in findings indicating trade of commodities such as wine and olive oil (Willems, 1986). Such shipping networks, and the (presumably) associated harbour (Driessen, 2007), suggest that river migration dynamics would have played an important role in their settlement location, and may explain their westward movement.

METHODOLOGY

Lithological borehole descriptions

Two borehole transects (A and B) were delineated across the study area (Fig. 3). Transect A is 1785 m long, has a north-west/south-east orientation and is positioned perpendicular to the scroll bar morphology (and hypothesized counterpoint-bar deposits) visible in the DEM in Fig. 3. Transect B is 2175 m long, and has a south-west/north-east orientation across the hypothesized counterpoint to point bar transition, where a gradation of finer counterpoint to coarser point-bar deposits is expected. A total of
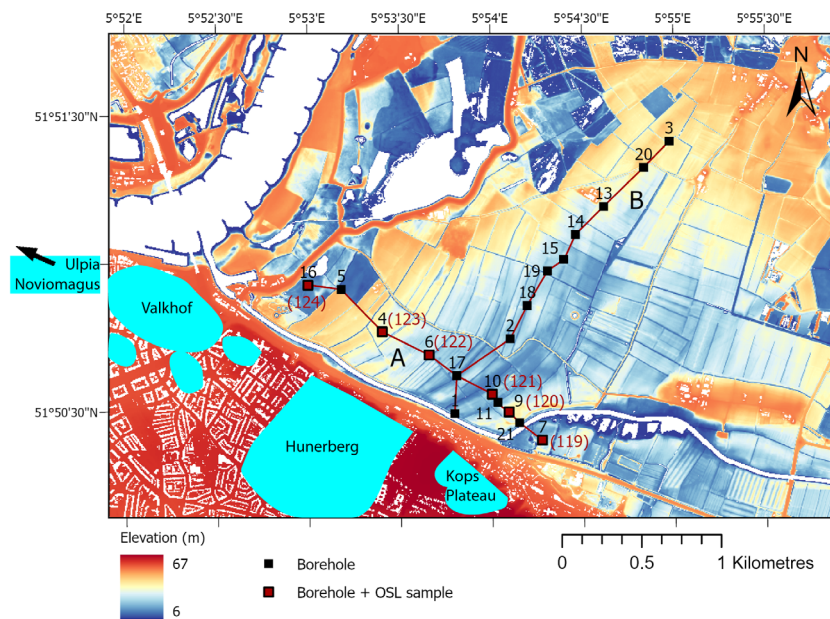
Fig. 3. Digital elevation map (Algemeen Hoogtebestand Nederland 3) showing the locations of transects A and B (labelled), and the numbered borehole locations and optically stimulated luminescence (OSL) sampling sites. Main Roman military camps and settlements (adapted from Willemse, 2019) discovered in Nijmegen atop the ice-pushed ridge are shown in light blue.

19 boreholes were made, with each transect consisting of ten boreholes (one borehole overlaps both transects). Borehole locations were dependent on where permission by the landowners was given to access their land, and therefore the distances between boreholes varies. Depths of boreholes ranged between 3.2 m and 6.3 m. Across the potential palaeochannel in Transect A and in the middle of Transect B where the hypothesized inflection point lies, spacing between boreholes was less than across the rest of the transect.

The surface elevation and location of each borehole site was measured using RTK (real time kinematic positioning)–GPS (horizontal and vertical accuracy ±1 cm). Boreholes were made using an Edelman auger (unsaturated sand), a gouge auger (clay) or a Van der Staay suction corer (saturated sand), depending on the type of sediment encountered. Descriptions of each borehole were made for 10 cm intervals using the procedure of Berendsen & Stouthamers (2000) and the Dutch classification system (de Bakker & Schelling, 1989), including texture, median sand grain size (if applicable), OM (organic matter) content, plant material, colour, gravel (>2 mm) content, Ca content and oxidation/reduction mottling. Sand grain size was measured in the field by visual comparison with a sand ruler. Additional observations such as layering or distinct differences within the 10 cm interval were also recorded.

Borehole data was plotted in the programme LLG 2012 (Cohen, 2012) and used to draw lithological cross-sections of the sub-surface across transects A and B. Based on lithological characteristics, several facies were then identified and described. Interpretation of their lithogenesis took into account the depositional environments associated with these lithologies, stratigraphic relationships, the OSL dating results and the surface morphology.

Optically stimulated luminescence dating

Optically stimulated luminescence (OSL) dating measures the luminescence signal that accumulates in buried quartz grains due to naturally occurring radioactivity. As light exposure resets the OSL signal, OSL dating determines the time since the sediment was exposed to light (Preusser et al., 2008). The method is widely applied to fluvial deposits (e.g. Wallinga, 2002; Rittenour, 2008). To determine the burial age, the natural OSL signal is compared to signals induced by laboratory-administered doses on small subsamples (aliquots) to estimate the equivalent dose (D_e, Gy). The palaeodose (Gy), defined as best-estimate of true burial dose, is obtained through statistical interpretation of the D_e distribution. In addition, the yearly absorbed radiation dose (dose rate, Gy/ka) is calculated from radionuclide activity concentrations, taking into account water content and burial depth. An

OSL age is then calculated as follows: age (ka) = palaeodose (Gy)/dose rate (Gy/ka). This method is increasingly used to date fluvial sediments because a lack of *in situ* organic material can lead to age over-estimation (in case of transported material) or underestimation (in case of bioturbation) in the traditionally used radiocarbon dating (Wallinga, 2002). OSL dating can determine the time of deposition with a relative precision of 4 to 5% at best (at 1σ; Wallinga & Cunningham, 2014).

OSL sampling

Six samples were collected for OSL dating within transect A (Fig. 3) to establish the direction of accretion of the scroll bar deposits, and thus the direction of channel migration. Sample locations and depths were decided upon following the lithological borehole descriptions to ensure that sufficiently thick sand layers required for OSL were present (Preusser et al., 2008). Samples were taken below minimum groundwater levels to ensure that moisture levels were most representative of average conditions since deposition, minimizing uncertainty when calculating the environmental dose rate. Sample depths ranged between 2.2 m and 4.5 m below surface level [5.64 to 7.68 m + NAP (Normaal Amsterdams Peil/ Amsterdam Ordnance Datum)]. The horizontal distance between samples ranged between 160 m and 560 m. One of these samples (NCL2321-119) was taken to identify the boundary of the study area and was expected to form part of a river terrace deposit from the Late Pleistocene or Early Holocene (Cohen & Stouthamer, 2012; Willemse, 2019). Samples were taken using a Van der Staay suction corer following the method of Wallinga & Van der Staay (1999), using 30 cm PVC tubes, flexible lids and tape to seal the samples and prevent light exposure.

OSL measurements

Samples were analysed in The Netherlands Centre for Luminescence dating (NCL). The outer 3 cm of material in the sampling tubes was removed under safelight conditions and prepared for dose rate estimation (see below). The 212 to 250 μm quartz fraction of the remaining material was prepared for luminescence measurements. Samples were sieved, treated with HCl (10%) to remove carbonates, H_2O_2 (10%) to remove organic matter (OM), then passed through a Frantz LB-1 Magnetic Barrier Laboratory Separator (S.G. Frantz Co., Tullytown, PA, USA) to obtain a purer quartz sample. Subsequently, samples were treated with HF (40%) to dissolve feldspars and etch the quartz grains, rinsed with HCl and re-sieved to remove grains which were partly dissolved due to HF treatment. OSL measurements were measured on either a Risø TL/OSL DA15 reader delivering 0.1217 Gy/s, or a Risø TL/OSL DA20 reader delivering 0.1447 Gy/s at the sample position, both equipped with blue diodes and a Sr/Y beta source. The single aliquot regenerative dose (SAR) protocol by Murray & Wintle (2000) was used for D_e measurement (Table S1). Preheat and cut-heat temperatures of 200°C and 180°C were selected based on thermal transfer tests (Truelsen & Wallinga, 2003). A minimum of 21 aliquots per sample were measured, using a mask size of 2 mm, resulting in approximately 75 grains per aliquot. Measurements were analysed using Risø Luminescence Analyst software using an early background subtraction protocol of Cunningham & Wallinga (2010). Rejection criteria included the error on the test dose response (>10%), recuperation (>10% of highest regenerative dose response), feldspar contamination (IR signal >10% of OSL signal) and recycling (>10% from unity).

Dose rate estimation

The material separated for dose rate estimation was dried and combusted to measure water and organic matter (OM) content. Subsequently, samples were ground and sieved over 300 μm, then mixed with wax to form pucks of 2 cm thickness. The pucks were analysed using high-resolution gamma ray spectrometry for activity concentrations of ^{40}K, U and Th decay chains (Table S2). Attenuation of radiation due to moisture and OM content were accounted for following the method of Aitken (1998). Water content of sandy samples was assumed to be 20 ± 3% by weight corresponding to the average porosity of sand being 34% (Wallinga & Bos, 2010). Sample NCL-2321120 was noted to have higher clay content, and therefore the measured water content was used (32.5%) for this sample to calculate dose rate attenuation by water, albeit with a larger uncertainty of 7.5%. Measured OM contents were used for the calculation of dose rate attenuation by OM, assuming a relative error of 10%; these values were all below 2% (Table S2). Cosmic ray contribution to dose rate was calculated based on Prescott & Hutton (1994), assuming instant burial to present depth below surface for all samples (Table S3).

Age estimation

Given the requirement of luminescence dating for a grain's OSL signal to be completely reset, using OSL to date fluvial sediments could arguably be unsuitable due to limited light exposure in some fluvial settings (Wallinga, 2002). To account for potential heterogenous bleaching in Late-Holocene samples, a bootstrapped minimum age model (bsMAM; Galbraith *et al.*, 1999; Cunningham & Wallinga, 2010) was applied to the D_e measurements to identify a minimum dose that is assumed to represent the dose of a well-bleached, or fully reset signal (Chamberlain *et al.*, 2018). A required parameter for the MAM is the overdispersion, or σ_b (representing expected variation in D_e estimates beyond the measurement uncertainty, for example, due to dose rate heterogeneity) of a well-bleached sample. Since the degree of bleaching in the samples is not known, a calculated σ_b was used following the procedure of Chamberlain *et al.*, (2018). This approach assumes that at least some of the samples are well-bleached and provides insight in overdispersion for well-bleached samples. The procedure involves running a bootstrapped central age model (CAM; Galbraith *et al.*, 1999) on each sample to obtain the overdispersion per sample and subsequently running a bsMAM (with σ_b of 0) on the resultant overdispersion values. The output provides the best estimate of expected overdispersion for well-bleached samples, and is then used as input to run the bsMAM for each individual sample. The calculated σ_b used was $11 \pm 5\%$, which is in agreement with expected overdispersion for 2 mm aliquots (Cunningham *et al.*, 2011). For sample NCL-2321119, expected to be of Late-Pleistocene or Early-Holocene age, heterogeneous bleaching is of less concern given that potential offsets due to poor bleaching are much smaller compared to the depositional age of the sample. To avoid bias by outliers, the palaeodose for this sample was derived from the mean of the D_e distribution after iterative removal of estimates deviating more than two standard deviations from the mean.

Channel migration direction and rate

The OSL ages obtained on the scroll bar deposits are used to determine the migration direction and migration rate of the channel. Towards this, OSL ages obtained for samples NCL-2321120 to NCL-2321124 are plotted as a function of the distance from the present

channel and the migration rate is then obtained through a weighted linear regression through these datapoints. The limited amount of data does not allow more advanced fitting, and the uncertainties on the individual ages prevents meaningful estimates of migration rate between two samples. For the fitting, only unshared errors of the OSL ages are taken into account (see e.g. Rhodes *et al.*, 2003). The thus obtained slope of the line provides the migration rate (m/year). The total uncertainty on this number is obtained by combining the error obtained from the weighted linear fit, with the relative age uncertainties shared by all samples (for example, calibration of instruments; total 3.5% of age).

RESULTS

Borehole cross-sections

Two lithological cross-sections were created based on the borehole descriptions of transects A and B (Figs 4A and 5A). Several facies were identified within the lithological cross-sections A and B by analysing grain-size trends and relative positioning of the deposits, as well as characteristics noted in the field. Table 1 provides a summary of these facies.

Facies 1, in the south-east of cross-section A (Fig. 4), is subdivided into Facies 1a and 1b. Facies 1a is comprised of a clear fining-up sequence that is lacking in the rest of the study area. This sequence consists of non-calcareous medium to coarse-grained coloured sands (210 to 1000 μm) that are in places poorly sorted within their 10 cm interval grain-size classification. Facies 1a is topped by Facies 1b: a thick (±2 m) layer of non-calcareous heavy clay.

Facies 2 is volumetrically the most significant facies in cross-section A (Fig. 4) and consists predominantly of fine material. It has been subdivided into Facies 2a, 2b and 2c based on lithology and additional distinguishing characteristics. Facies 2a is a well-sorted, fine–medium grained (150 to 300 μm) narrow body of sand at the base of cross-section A, resting directly on top of Facies 3. Facies 2a is calcareous and contains some plant material throughout the base of the sequence. Surrounding Facies 2a and making up most of the lower depths of cross-section A is Facies 2b, consisting of silty and sandy clays with frequent occurrences of thin (<3 cm) sand layers and sporadic occurrences of slightly
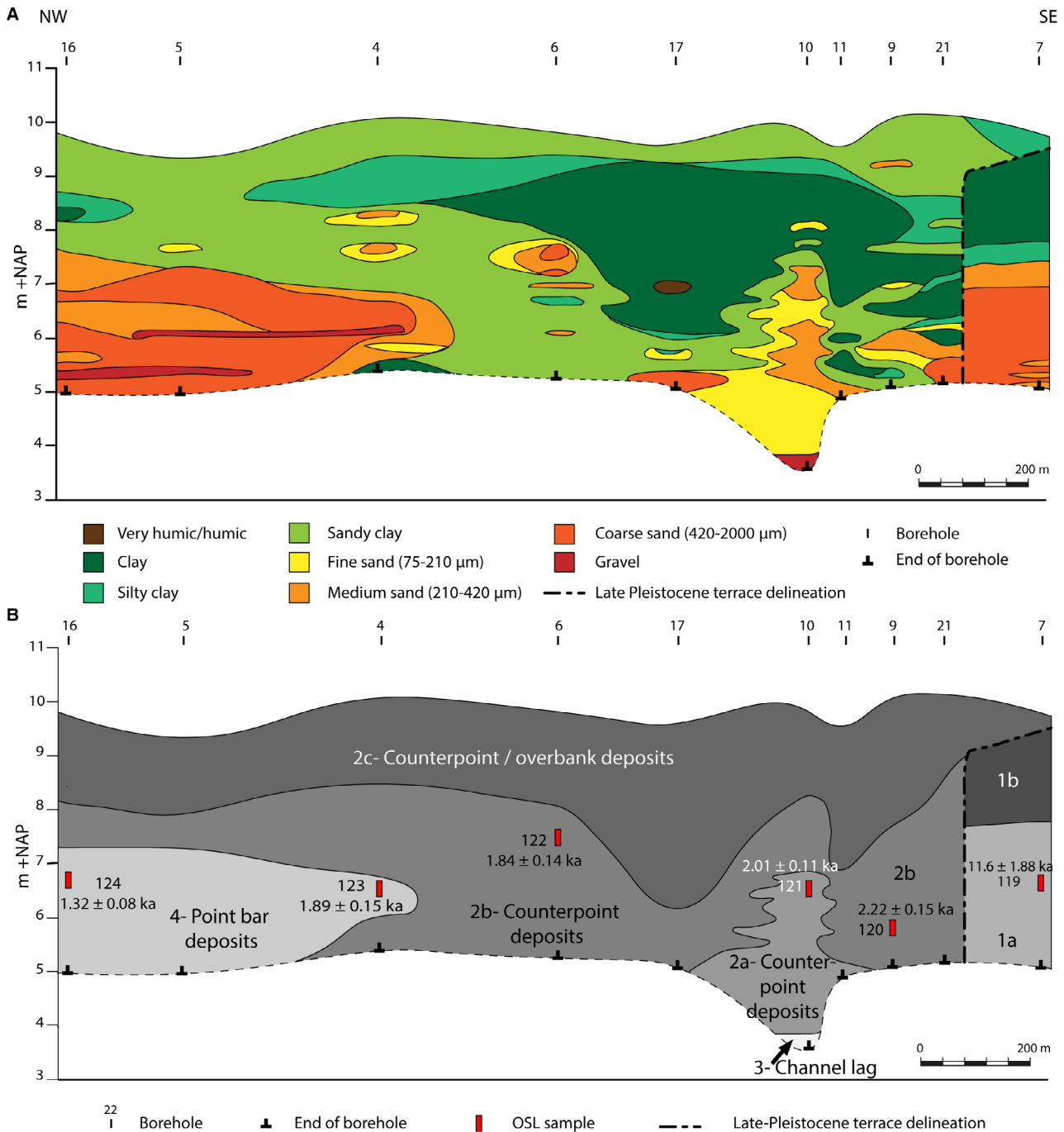
Fig. 4. (A) Lithological cross-section for transect A. (B) Distribution of identified facies in cross-section A (numbered; refer to Table 1 for descriptions; NAP, Normaal Amsterdams Peil/Amsterdam Ordnance Datum). Optically stimulated luminescence (OSL) sample locations are given with their abbreviated numbers (all preceded by NCL2321) and with the obtained ages.

larger sand bodies (75 to 420 µm) throughout. Facies 2b is calcareous and contains some plant material. This facies is also present at the base

of cross-section B (Fig. 5) as a thick (±3 m) sequence of material in the south-west, gradually thinning and phasing out towards the centre
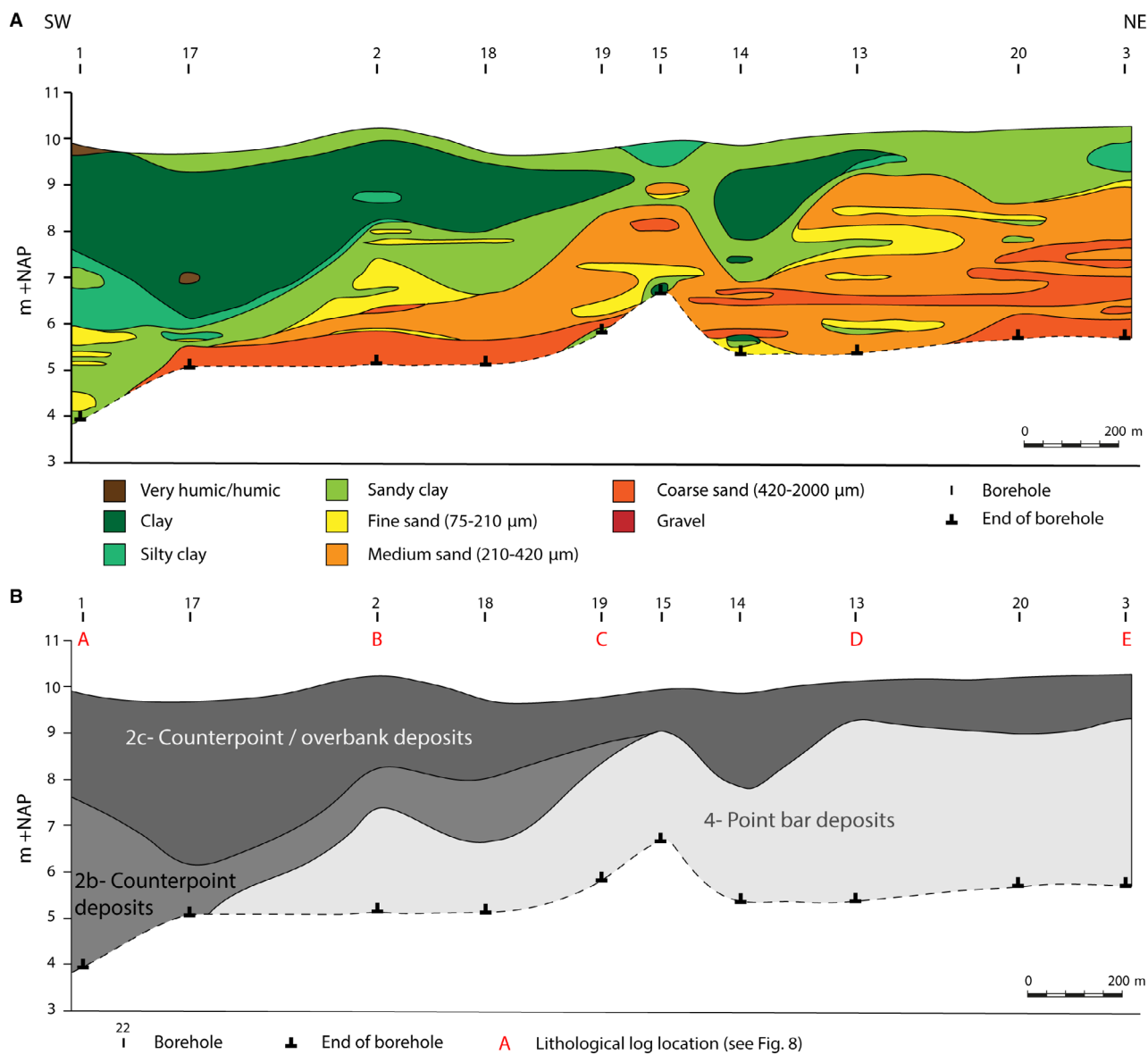
Fig. 5. (A) Lithological cross-section for transect B. (B) Distribution of the identified facies in cross-section B (numbered; refer to Table 1 for descriptions) and locations of lithological logs shown in Fig. 8.

of the cross-section. The fine-grained material making up the upper 1 to 3 m of sediments in cross-sections A and B belongs to Facies 2c. This facies is characterized by homogenous heavy clays, silty clays or sandy clays, which may be slightly humic and can contain plant material. Facies 2c is variably calcareous, with the boreholes that contain more heavy clays often being less calcareous or non-calcareous (Figs S1 and S2).

Facies 3 is only encountered once and consists of fine (5 to 16 mm) well-rounded gravels

found at 6.0 to 6.3 m depth in borehole 10 (Fig. 4). This facies directly underlies Facies 2a, with a sharp transition from fine sand to gravel.

Facies 4 is present in both cross-sections (Figs 4 and 5). In the base of cross-section A this facies is present in boreholes 16 and 5 as medium to coarse (210 to 2000 μm) calcareous sands up to 2.4 m thick. Gravelly sand and gravel layers occur frequently. In cross-section B, Facies 4 is volumetrically the most significant facies, present as a several-metres-thick sequence at the base of the cross-section in the north-east, gradually thinning

Table 1. Descriptions and interpretations of the identified facies (see also Figs 4 and 5 for facies distribution within cross-sections).

Facies		Lithology	Interpretation/lithogenesis
1	a	Poorly sorted non-calcareous medium–coarse sands (210 to 1000 μm) with a well-developed fining-upward sequence	Late-Pleistocene terrace deposits
	b	Non-calcareous heavy clay	Pre-Roman overbank deposits
2	a	Fine–medium well-sorted calcareous sands (150 to 300 μm)	Counterpoint deposits
	b	Clay and silty/sandy clays with distinct bands of fine to medium sands throughout. Calcareous	Counterpoint deposits
	c	Homogenous heavy clays, light clays and sandy clays. Variably calcareous	Counterpoint deposits/ overbank deposits
3		Well-rounded gravels up to 1 cm diameter	Channel-lag
4		Fine to coarse calcareous sands (150 to 2000 μm). Gravelly and/or gravel layers at greater depths. Occasional distinct layers of plant material and clay layers/mud clasts	Point-bar deposits

out as Facies 2 overlying this sequence thickens towards the south-west (Fig. 5B). Facies 4 varies in grain size from fine to coarse-grained (150 to 2000 μm), sporadically containing up to 25% gravel. Clay layers, mud clasts and distinct layers of plant material are found throughout this facies to the north-east of transect A.

Optically stimulated luminescence results

The OSL results calculated using a bootstrapped minimum-age model (bs-MAM) are presented in Table 2 and in Fig. 4B. Despite the expectation that poor bleaching may have affected burial dose estimates, samples appeared to be overall well-bleached, demonstrated by D_e distributions with low overdispersion and a general overlap of the age distributions seen within the bsMAM and CAM models (Fig. S3). The samples from the Late-Holocene fluvial deposits in transect A date from 2.22 ± 0.15 ka furthest from the present river (sample NCL-2321120) to 1.32 ± 0.08 ka closest to the present river (sample NCL-2321124).

As expected, sample NCL-2321119 (borehole 7) is much older than the other samples, with an age of 11.6 ± 0.5 ka, confirming the presence of a Late-Pleistocene fluvial terrace at this

Table 2. Quartz optically stimulated luminescence (OSL) dating results calculated using the bootstrapped minimum-age model (bs-MAM).

	Coordinates (RD new)		Sample elevation	Palaeodose (Gy)		Dose rate (Gy/ka)		OSL age (ka)		
Sample	x	y	(m + NAP)	μ	σ	μ	σ	μ	σ	OSL age (BCE–CE)
NCL2321-119	190 619	427 948	6.65	14.78	3.00	1.62	0.06	9.13	1.88	8988 BCE–5224 BCE
NCL2321-120	190 410	428 124	5.73	3.79	0.15	1.71	0.09	2.22	0.15	342 BCE–50 BCE
NCL2321-121	190 304	428 235	6.53	4.06	0.18	2.01	0.07	2.01	0.11	108 BCE–122 CE
NCL2321-122	189 908	428 481	7.53	3.28	0.22	1.78	0.06	1.84	0.14	38–316 CE
NCL2321-123	189 614	428 627	6.75	2.66	0.19	1.41	0.05	1.89	0.15	19 BCE–285 CE
NCL2321-124	428 918	189 146	6.44	2.17	0.11	1.64	0.06	1.32	0.08	618–776 CE

location (Mulder, 1989; Cohen et al., 2012; Willemse, 2019).

Channel migration direction and rate

The migration rate of the channel (Fig. 6) was calculated as 1.93 ± 0.39 m/year in the northwest direction (Fig. 6). OSL ages of four out of five samples agree with the linear trendline within their individual unshared error 1σ uncertainty, and all agree within 2σ (not shown), indicating that the linear trendline provides a good fit. Due to overlapping error margins, the apparent migration rate between individual samples would not provide meaningful estimates, as evident from opposing directions to actual migration for some sample combinations (Table S4).

Lithofacies interpretation

The lithofacies identified in transects A and B have been interpreted in the context of the fluvial nature of the study area, taking into account the surrounding topography, surface morphology, chronology established by the OSL results and the relative positioning of the different facies within the two cross-sections. Figure 7 shows a simplified map of the interpretation of the study area.

Facies 1a and 1b are identified as Late-Pleistocene terrace deposits and pre-Roman overbank deposits respectively. The borehole in which this facies is identified (borehole 7) falls within the delineation of a Late-Pleistocene terrace remnant east of the Ooijpolder (Fig. 7), with previous research confirming the presence of this river terrace (Mulder, 1989; Cohen & Stouthamer, 2012; Willemse, 2019). Despite their lithological differences, Facies 1a and 1b are classed in the same facies in order to distinguish older deposits from the Late-Holocene-aged deposits of interest in this study.

Facies 2, which forms most of cross-section A running parallel to the ice-pushed ridge (Fig. 4), is interpreted as counterpoint deposits (Facies 2a, 2b and 2c), grading upward into overbank deposits (Facies 2c). The dominantly fine-grained (Facies 2a) and clayey (Facies 2b and c) lithologies found through much of the cross-section suggest a relatively low-energy depositional environment, with some variability which accounts for its non-homogeneity. This relatively fine grain size indicates deposition likely to be sourced from suspension. The thickness of Facies 2 (up to 5 m) excludes the possibility of this facies being comprised of solely overbank deposits when considering reconstructed Late-Holocene channel geometries that estimate the Waal to have been around 6 m deep (Willemse, 2019). Counterpoint deposits have been found to be potentially as thick as point-bar deposits (Smith et al., 2009, 2011), which in the present study area appears also to be the case given the stratigraphic relationship with Facies 3. The depth at which Facies 3 is located and its
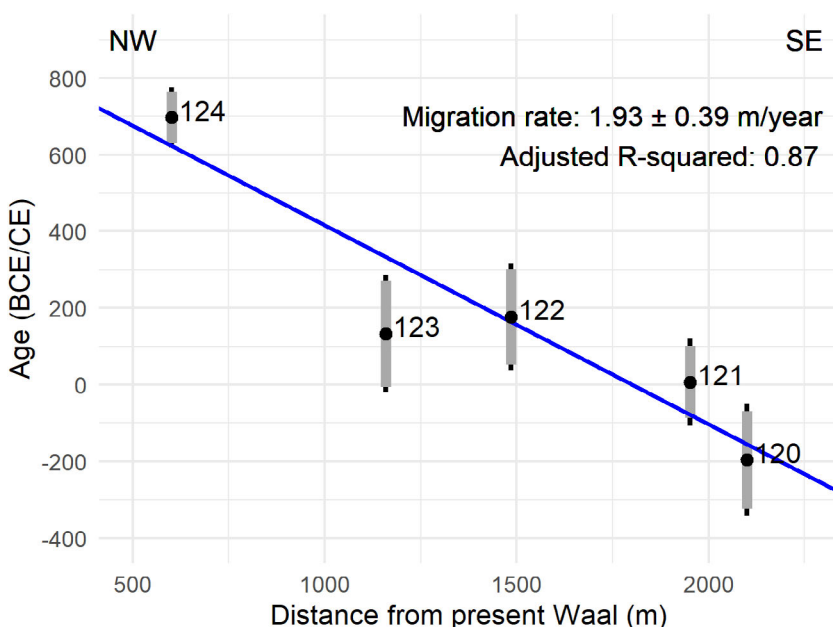

Fig. 6. Results of optically stimulated luminescence (OSL) dating for samples NCL-2321120 to NCL-2321124 plotted as age over distance. Grey error bars show 1σ uncertainty calculated using unshared errors only; black error bars include systematic uncertainty shared by all samples. Numbers indicate the OSL sample number (all preceded by 'NCL-2321'). Blue line shows the weighted linear regression fit corresponding to a migration rate of 1.93 m/year.
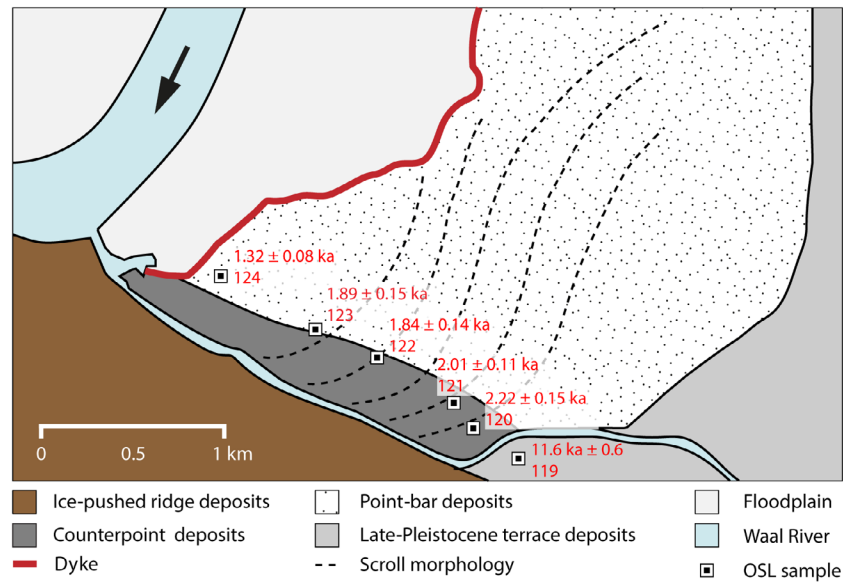
Fig. 7. Interpreted map of the study area (see Fig. 2), with optically stimulated luminescence (OSL) ages and sample numbers (all preceded by 'NCL-2321').

agreement with reconstructed geometries, as well as the characteristic gravel lithology (Fig. 4A), leads to this facies being interpreted as channel lag. With Facies 2 directly overlying the channel lag, its thickness equals at least that of any associated point bar. Furthermore, sediments in Facies 2, particularly Facies 2b, concur with descriptions of counterpoint stratigraphy typically being clayey/silty, with occasional sand lenses comprising <20% of the total sedimentary unit (Smith *et al.*, 2009). Despite Facies 2a being sandy (Fig. 4A), it is not uncommon for localized sand lenses to occur; for example Smith *et al.* (2011) found a sand to gross stratigraphy percentage of up to 45% in a core of a counterpoint-bar deposit in the Peace River, Alberta, Canada. Nanson & Croke (1992) describe counterpoint deposits as unique among floodplain deposits in that their deposition of fine-grained sediments is a result of localized rather than overall low-energy environments. Such localization can then also be expected to yield sediments that contain some heterogeneity in grain size across the entire transect, as observed in Facies 2a compared to the rest of Facies 2 (Fig. 4A).

The surface morphology seen in the DEM further supports this interpretation, showing concave scrolls pointing upstream relative to the current location of the Waal (Fig. 2B). These are in agreement with the typical orientation of those of counterpoint deposits, which arc in the upstream direction (Smith *et al.*, 2009). Meanwhile, the OSL results indicate a south-east to north-west direction of accretion, with older sediments being found farther from the river. This would be expected for counterpoint deposition, given that migration takes place in a downstream direction, towards the river's present location. These findings exclude the possibility of point-bar formation and channel migration to the south-east followed by channel cut-off near the rivers present position having taken place, because for that scenario it would be expected that the chronology is reversed.

Facies 4 is interpreted as point-bar deposits, with its occasional gravel, silt/clay and plant material layers matching descriptions of typical point-bar lithologies (Allen, 1965; Nanson, 1980). The lithologies of Facies 4 and 2, and their stratigraphic relationship – a thick sequence of Facies 4 in the north-east of cross-section B gradually thinning out to the south-west where Facies 2 thickens – are typical for point-bar – counterpoint-bar transitions (Sylvester *et al.*, 2021), as is the S-shaped surface morphology seen in the DEM (Fig. 2B; see Makaske & Weerts, 2005; Smith *et al.*, 2009, 2011; Durkin *et al.*, 2020). This point-bar – counterpoint-bar transition can also be seen in the lithological logs of several boreholes across Transect B, where sandy sediments of Facies 4 dominate the profile in the north-east farthest from the ice-pushed ridge, with Facies 2 becoming dominant closer to the ice-pushed ridge farther south-west (Fig. 8). Facies 2c is the only component of Facies 2 extending all the way across cross-section B, consisting solely of fine overbank
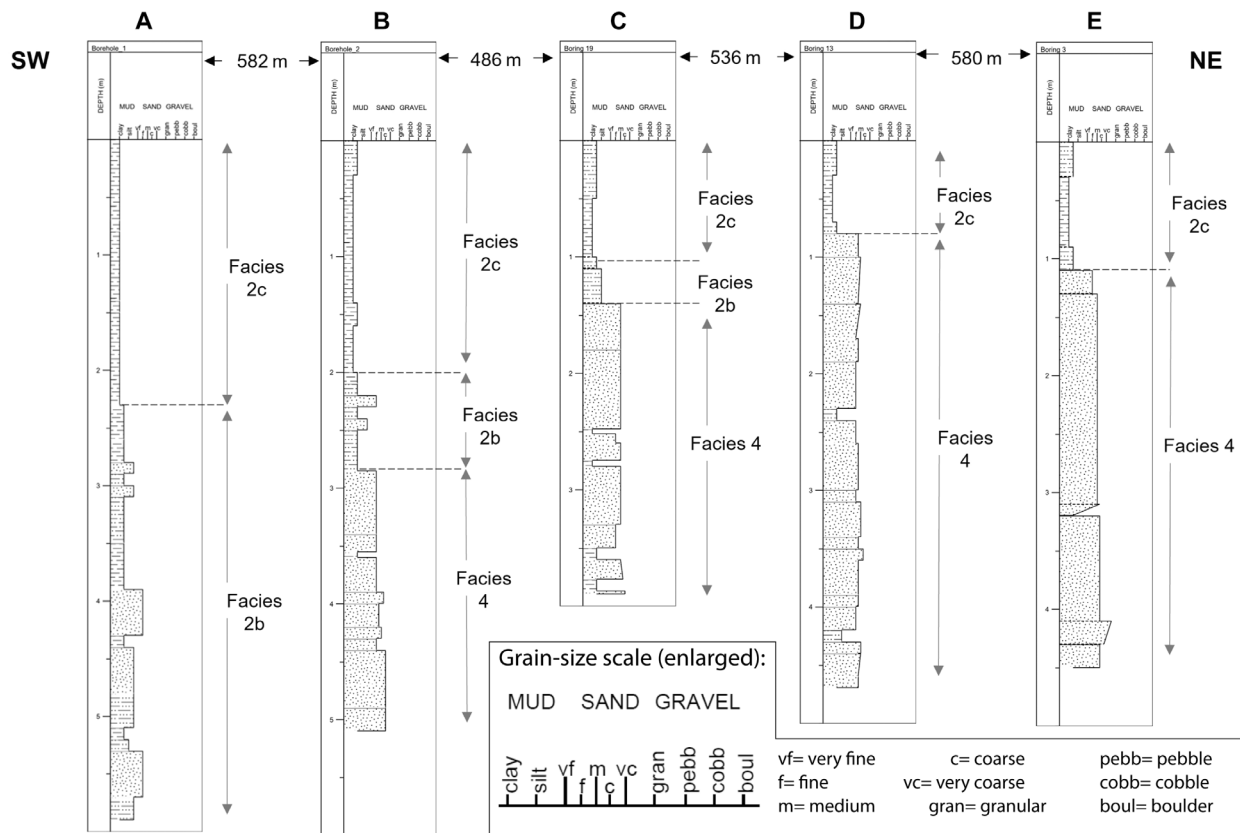
Fig. 8. Sedimentary logs from boreholes in transect B showing the transition from counterpoint-bar deposits (south-west) to point-bar deposits (north-east). For borehole locations refer to Fig. 5B.

deposits typically found on a point bar sequence in the north-east half of the transect.

A definitive boundary between the identified counterpoint and point bars is difficult to ascertain (despite those given by the facies classifications), but the inflection point at the counterpoint – point-bar transition is considered to have been between boreholes 17 and 2 in cross-section B. Here, the variability in grain size that separates the different facies should not be a deciding factor to define one deposit or the other, but rather should be considered as a part of this transition zone. Indeed, observations made in the field in borehole 17 show large variations in grain size. Different depositional mechanisms responsible for counterpoint deposition can potentially explain some of this variability (see discussion on *Depositional mechanisms*).

Facies 4 is also identified in the north-west part of cross-section A, and is interpreted here as the downstream end of the adjacent point bar approaching the inflection point and transition to counterpoint bar. Deposits in the north-west

of cross-section A were observed farther away from the ice-pushed ridge compared to in the south-east of the cross-section (355 m and 175 m, respectively). The associated counterpoint deposits that lie adjacent to, and over Facies 4 are located slightly farther upriver and closer to the inflection point than they are in the south-east part of the cross-section. Therefore they could be expected to be thinning out over Facies 4 as part of the transition zone compared to the thicker deposits where the river reaches maximum curvature in the south-east, i.e. closer to the ice-pushed ridge. Smith *et al.* (2009) found a similar trend in their studies of the Peace River where several profiles were made across each counterpoint bar, with those profiles closer to the inflection point showing thinner layers of silty counterpoint deposits. This would indicate that Facies 4 consists of the downstream end of the point bar lying adjacent to the counterpoint deposits directly beneath the ice-pushed ridge. Chronologically this agrees with the OSL findings, since accretion in the

associated point bar would take place in the same direction as that of the counterpoint bar, just farther upstream.

DISCUSSION

Opportunities and limitations

This research identifies counterpoint deposition to have taken place in a Late-Holocene aged bend in the Waal River, where previous palaeo-geographical reconstructions for depositional events in the Ooijpolder assumed lateral migration by point-bar formation and meander bend cut-off (Cohen *et al.*, 2012; Willemse, 2019; Heunks & van de Geer, 2021). The combination of lithofacies interpretation and reconstruction of migration direction using OSL dating conclusively confirmed the hypothesis for downstream migration of the river bend by counterpoint deposition. Given the inherent variability of counterpoint deposits as encountered here and in other studies (e.g. Smith *et al.*, 2009, 2011; see also discussion on *Depositional mechanisms* below), the chronological constraints on channel migration direction provided indispensable evidence of the existence of counterpoint bars. Indeed, Makaske & Weerts (2005) concluded that counterpoint bars can easily be mistaken for deposits from point bars, natural levées or residual channels.

Previous studies (Rodnight *et al.*, 2005; Candel *et al.*, 2018; Quik & Wallinga, 2018) have employed OSL dating for the reconstruction of lateral migration rates of meander bends through point bar formation. Here, it is shown for the first time that the method is also applicable to distinguish counterpoint bars from conventional point bars, and that migration rates can also be determined provided that sufficient samples are dated. If migration rate is based on too little data, it may yield inaccurate or even wrong results (Table S4).

Depositional mechanisms

Despite having established that counterpoint deposits are present in the study area, some uncertainty still exists concerning the mechanism of deposition, especially considering the variability in the deposits encountered. Several mechanisms of counterpoint deposition have been described, which are summarized in three distinct processes as follows:

1 Reverse flow in bends at angles close to or greater than 90° can scour deep pools into the outer bank of the river that get filled with a thick sequence of fine sand with a relatively high silt content (eddy accretion deposit; Smith *et al.*, 2009; Fig. 9A).

2 Page & Nanson (1982) describe flow expansion and separation taking place following deflection of the flow around the upstream point bar, causing erosion of the opposite convex bank and resulting in widening of the bend (Fig. 9B). With this mechanism, the availability of sufficient suspended material compared to bedload is necessary for infilling of the outer part of the bend (Makaske & Weerts, 2005). The condition for sufficient suspended material seems to be met in the Lower Rhine River (Erkens *et al.*, 2006).

3 Counterpoint deposition can also be related to the weakening of helicoidal currents downstream of point bars, where a slack water zone develops (Nanson, 1980), resulting in diffusion and deposition of suspended sediment towards the concave bank (Nanson, 1980; Makaske & Weerts, 2005; Fig. 9C).

Given the variability encountered within the counterpoint deposits identified in this study, it is likely that multiple mechanisms can be attributed to their formation. Mechanism 1, where a scoured pool is filled by sandy eddy accretion deposits, is considered the least likely. Eddy accretion deposits have been described to be very thick as a result of deep scouring, and can be up to twice as thick as adjacent point-bar deposits (Smith *et al.*, 2009), which in the current study area cannot be verified because a channel lag was only encountered in one location. However, the relatively shallow depth of 6 m at which channel lag was encountered (Fig. 4), which is in agreement with reconstructed channel geometries (Willemse, 2019), does not indicate deep scouring to have occurred. The relatively fine-grained material encountered in Transect A also speaks for a lower-energy depositional environment than that in which eddy-accretion deposits form. Furthermore, the angle at which the river met the ice-pushed ridge is notably less than the near-90° where eddy accretion deposits form, as described by Makaske & Weerts (2005) and Smith *et al.* (2009). Based on the scroll bar morphology (Fig. 2), this angle is estimated to be between 45° and 70°.

Mechanism 2, facilitated by flow expansion causing recirculation of flow in the outer bend
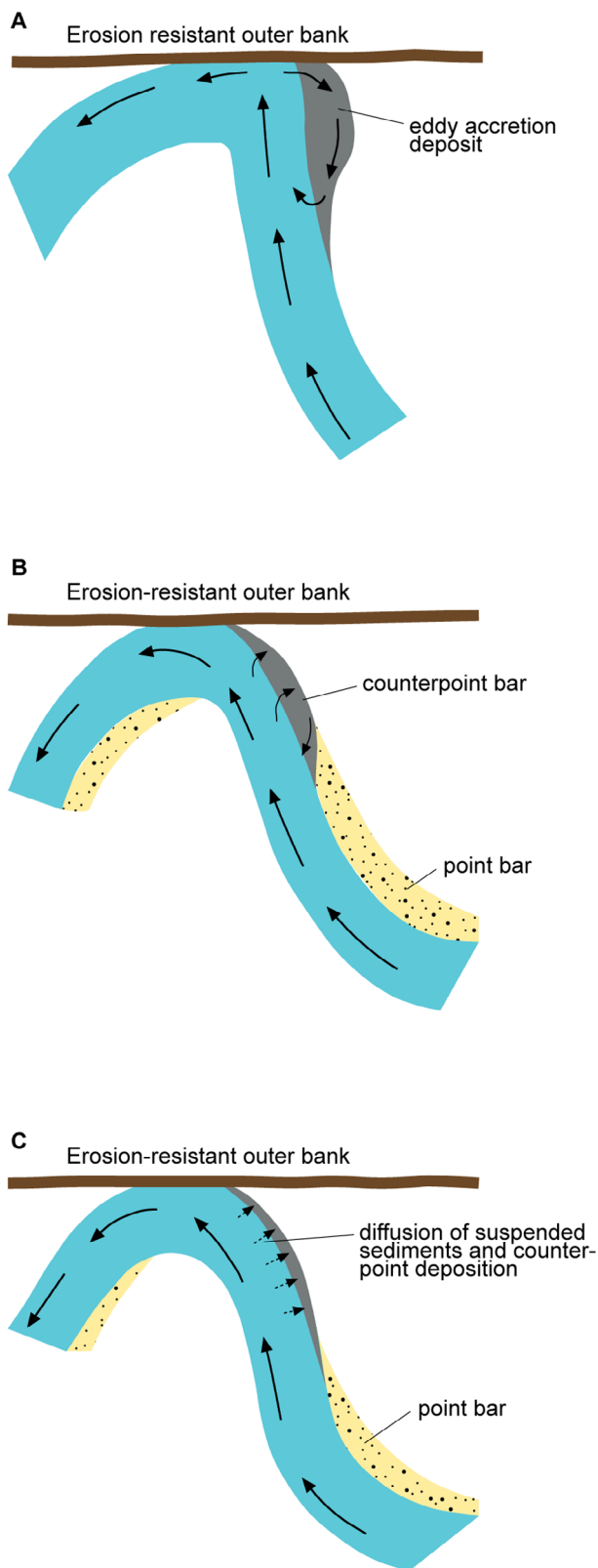
Fig. 9. Schematic figure of various depositional mechanisms for counterpoint bar formation (adapted from Makaske & Weerts, 2005).

of the river, could plausibly explain some of the variation seen in the study area. Page & Nanson (1982) described the forming of benches in the outer bend by secondary currents, comprised of basal medium to fine sands and topped with much finer-grained deposits containing silts, clays and organics. This description matches the lithologies identified in borehole 10 in cross-section A (Facies 2a overlain by Facies 2b), and between boreholes 2 and 17 in cross-section B (Facies 4 overlain by Facies 2b; Figs 4 and 5). However, for this to have been the prevailing depositional mechanism, it could be expected that some discontinuity in the scroll bar morphology would be visible as a result of recirculating flow, which is not the case. Changes in sediment supply or discharge could also account for the observed variability in grain size, for example by human influence upstream of the study area. Although dyke construction around the Waal River took place centuries after Roman occupation, there is other evidence that the Romans also modified the fluvial system. Upstream of the study area, a Roman dam was built around 12 BCE during their early occupation at the bifurcation of the Waal and the Nederrijn (Fig. 2A; Verhagen et al., 2017) in an attempt to make the latter more accessible for ships (Willems, 1986; van den Broek et al., 2009). This dam was removed in 70 CE to restore the original discharge volumes to the Waal (van den Broek et al., 2009). A reduction in discharge of the Waal with building of the dam and subsequent increase in discharge with its removal may have influenced the migration rate and sediment load capacity of the river. It could be speculated that the lithological variation in cross-section A seen between Facies 2a (borehole 10, OSL sample NCL-2321121) and the adjacent-lying Facies 2b may have been impacted by this fluctuating discharge. The OSL age of sample NCL-2321121 (108 BCE to 122 CE) in borehole 10 indeed encompasses the period within which the dam was built. This modification of the fluvial system may limit the validity of sedimentological comparisons of the identified counterpoint deposits with those in natural systems (e.g. Makaske & Weerts, 2005; Smith et al., 2009, 2011), and should be kept in mind when interpreting modern counterpoint deposits.

Diffusion of sediments in the counterpoint zone by mechanism 3 is considered the most likely depositional mechanism. Both the fine

grain size across most of transect A, and the S-shaped continuity of the surface scroll morphology from point bar to counterpoint bar speak for deposition by diffusion of suspended sediment. The variability seen in grain sizes across Facies 2a and 2b could also indicate episodes with varying depositional mechanisms, for example recirculating flow facilitated by mechanism 2 during periods of high discharge, or human influence affecting discharge and sediment volumes as described above.

Based on these observations, and those in other studies under various settings where different depositional mechanisms and sedimentary products exist (Page & Nanson, 1982; Makaske & Weerts, 2005; Smith *et al.*, 2009, 2011; Sylvester *et al.*, 2019), variability could be said to be an inherent characteristic of counterpoint deposits. Indeed Nanson & Croke (1992) emphasize that counterpoint deposition takes place due to localized, rather than overall low-energy conditions, suggesting that different products of this deposition are also likely to be found locally rather than as large, homogenous units.

Optically stimulated luminescence methodology and results

Despite potential challenges for OSL dating of fluvial sediments (Wallinga, 2002; Smedley & Skirrow, 2020), clearly heterogenous D_e distributions were not present in this study's samples, which points to the samples having been relatively well-bleached. A bsMAM was still applied to the Late-Holocene samples to avoid any bias related to heterogenous bleaching. The agreement between the CAM and bsMAM obtained ages for the Late-Holocene samples (Fig. S3), testifies to the well-bleached nature of these samples (Chamberlain & Wallinga, 2019).

It is tempting to relate the well-bleached nature of the samples to the low energetic nature of counterpoint-bar deposits. However, previous research suggested that the degree of OSL bleaching of fluvial deposits does not easily relate to the depositional environment, likely because the bleaching takes place during sediment transport rather than upon deposition (Wallinga *et al.*, 2010). The fine-grained nature of the counterpoint-bar deposits may suggest that they contain more suspended sediments than point-bar deposits, which could promote bleaching opportunities for the grains. However, there is conflicting evidence on the relationship between bleaching and grain size, with some studies

indicating that coarser grains are better bleached [reviewed in Smedley & Skirrow (2020)]. The grain size of 212 to 250 μm analysed here is relatively coarse and may not necessarily be representative for the overall more fine-grained nature of the encountered counterpoint deposits (Fig. 4). On the other hand, studies by Frings *et al.* (2014) indicate that this grain size is predominantly transported as suspended load in this part of the Rhine River, which could increase the likelihood of these sediments being well bleached. Another factor that may be of relevance to the well-bleached nature of samples is that they are deposited in a downstream reach of a large river system. Several studies have indicated progressive bleaching downstream (e.g. Guyez *et al.*, 2023), and previous work in the Holocene Rhine delta indicated relatively well-bleached OSL signals even for deposits formed in the past centuries (Wallinga *et al.*, 2010; Hobo *et al.*, 2014).

Implications

The identification of counterpoint deposition in a major channel of the Late-Holocene Rhine system of The Netherlands reveals the potential for these depositional processes to also have taken place in other parts of the Rhine-Meuse system, or in similar environments elsewhere. This study serves to demonstrate the potential prevalence of depositional processes that are not always associated with 'typical' meandering river systems and provides further insight into the increasingly apparent phenomenon of outer bank deposition in fluvial systems (e.g. Candel *et al.*, 2020; Sylvester *et al.*, 2021; Winkels *et al.*, 2022). The limited number of comparable studies in terms of the fluvial system, setting and time period indicates a knowledge gap on the subject, and highlights opportunities for further research to better understand the fluvial system and to inform spatial planning. Failure to recognize the complexity of fluvial processes and associated deposits may have implications for archeology (as demonstrated here), palaeo-geographical landscape reconstructions, river management and spatial planning, restoration and rewilding projects, as well as ecosystem functioning.

CONCLUSIONS

This study is the first to identify counterpoint deposits associated with a modern Rhine

distributary in The Netherlands. The deposits found beneath the scroll bar morphology along the Waal River branch of the Lower Rhine consisted of a thick sequence of fine, clay-dominated sediments that match published descriptions of counterpoint deposits. These sediments grade into sandier point-bar deposits farther upstream. The optically stimulated luminescence (OSL) ages obtained on the fine channel sediments indicate a downstream, rather than lateral, direction of sediment accretion, and thus channel movement. Based on the combined information on sediment composition and channel migration direction, it is concluded that the deposits are indeed counterpoint deposits. This demonstrates the potential of OSL dating to identify river migration direction and rate, and thus as a tool to identify counterpoint bar formation.

The results of this study have implications for the palaeogeographical reconstruction of the study area, because presently several different interpretations exist that assume point bar formation and associated lateral migration of the river bend. The occurrence of localized channel processes such as counterpoint deposition in the Waal River, however, also carries the implication that such processes may have taken place in other parts of the Rhine-Meuse delta and similar environments elsewhere. As well as affecting fundamental understanding of fluvial systems in The Netherlands, counterpoint deposition also has implications for river rewilding and restoration projects aiming to restore natural processes and enhance ecosystem functioning. Understanding of such river dynamics is crucial for river management and spatial planning in order to predict the behaviour of these more natural systems and to enable their successful restoration.

ACKNOWLEDGEMENTS

DATA AVAILABILITY STATEMENT

The data that support the findings of this study are available from the corresponding author upon reasonable request.

REFERENCES

Aitken, M.J. (1998) *Introduction to Optical Dating: The Dating of Quaternary Sediments by the Use of Photon-Stimulated Luminescence*, p. 267. Oxford University Press, Oxford, UK.

Allen, J.R.L. (1965) A review of the origin and characteristics of recent alluvial sediments. *Sedimentology*, **5**, 89–191.

Berendsen, H. (1982) De genese van het landschap in het zuiden van de provincie Utrecht (The genesis of the landscape in the Southern part of the province of Utrecht). *Utrecht Geograf. Stud.*, **25**, 1–259.

Berendsen, H. and **Stouthamer, E.** (2000) Late Weichselian and Holocene palaeogeography of the Rhine-Meuse delta, The Netherlands. *Palaeogeogr. Palaeoclimatol. Palaeoecol.*, **161**, 311–335.

Berendsen, H.J.A. and **Stouthamer, E.** (2002) Paleogeographic evolution and avulsion history of the Holocene Rhine-Meuse delta, The Netherlands. *Netherlands J. Geosci.*, **81**, 97–112.

Blanckaert, K. (2011) Hydrodynamic processes in sharp meander bends and their morphological implications. *J. Geophys. Res. Earth*, **116**, F101003. https://doi.org/10.1029/2010JF001806.

Candel, J.H.J., **Kleinhans, M.G.**, **Makaske, B.**, **Hoek, W.Z.**, **Quik, C.** and **Wallinga, J.** (2018) Late Holocene channel pattern change from laterally stable to meandering – A palaeohydrological reconstruction. *Earth Surf. Dyn.*, **6**, 723–741.

Candel, J.H.J., **Makaske, B.**, **Kijm, N.**, **Kleinhans, M.G.**, **Storms, J.E.A.** and **Wallinga, J.** (2020) Self-constraining of low-energy rivers explains low channel mobility and tortuous planforms. *Deposit. Rec.*, **6**, 648–669.

Carranza, C., **Onderwater, N.**, **Larsen, A.**, **Candel, J.**, **Bense, V.**, **Hoitink, T.**, **Wallinga, J.** and **van der Ploeg, M.** (2022) *Releasing the Banks: Initial Morphological Responses after Removal of Groynes and Installation of a Longitudinal Dam*. EGU General Assembly, Vienna.

Chamberlain, E. and **Wallinga, J.** (2019) Seeking enlightenment of fluvial sediment pathways by optically stimulated luminescence signal bleaching of river sediments and deltaic deposits. *Earth Surf. Dyn.*, **7**, 723–736.

Chamberlain, E.L., **Wallinga, J.** and **Shen, Z.** (2018) Luminescence age modeling of variably-bleached sediment: Model selection and input. *Radiat. Meas.*, **120**, 221–227.

Cohen, K. (2012) *LLG 2012 (Version 2.0.25) [Computer Programme]*. Utrecht University, Utrecht.

Cohen, K. and **Stouthamer, E.** (2012) Vernieuwd Digitaal Basisbestand Paleogeografie van de Rijn-Maas Delta: Beknopte toelichting bij het Digitaal Basisbestand Paleogeografie van de Rijn-Maas Delta.

Cohen, K.M., **Stouthamer, E.**, **Pierik, H.J.** and **Geurts, A.H.** (2012) Rhine-Meuse Delta Studies' Digital Basemap for Delta Evolution and Palaeogeography (Issue December). http://xn--persistentidentifier-ks2l.nl/?identifier=urn:nbn:nl:ui:13-nqjn-zl.

Cunningham, A.C. and **Wallinga, J.** (2010) Selection of integration time intervals for quartz OSL decay curves. *Quatern. Geochronol.*, **5**, 657–666.

Cunningham, A., **Wallinga, J.** and **Minderhoud, P.** (2011) Expectations of scatter in equivalent-dose distributions when using multi-grain aliquots for OSL dating. *Geochronometria*, **38**, 424–431.

De Bakker, H. and **Schelling, J.** (1989) Systeem van bodemclassificatie voor Nederland. *Grondboor & Hamer*, **20**, 210.

Driessen, M. (2007) *Bouwen om te blijven*. Universiteit van Amsterdam, Amsterdam.

Durkin, P.R., **Hubbard, S.M.**, **Holbrook, J.**, **Weleschuk, Z.**, **Nesbit, P.**, **Hugenholtz, C.**, **Lyons, T.** and **Smith, D.G.** (2020) Recognizing the product of concave-bank sedimentary processes in fluvial meander-belt strata. *Sedimentology*, **67**, 2819–2849.

Erkens, G., **Cohen, K.**, **Gouw, M.**, **Middelkoop, H.** and **Hoek, W.** (2006) Holocene Sediment Budgets of the Rhine Delta (The Netherlands): A Record of Changing Sediment Delivery. In: *Sediment Dynamics and the Hydromorphology of Fluvial Systems, Proceedings*, pp. 406–415. Dundee.

Frings, R., **Döring, R.**, **Beckhausen, C.**, **Schüttrumpf, H.** and **Vollmer, S.** (2014) Fluvial sediment budget of a modern, restrained river: The lower reach of the Rhine in Germany. *Catena*, **122**, 91–102.

Galbraith, R.F., **Roberts, R.G.**, **Laslett, G.M.**, **Yoshida, H.** and **Olley, J.M.** (1999) Optical dating of single and multiple grains of quartz from jinmium rock shelter, northern Australia: part i, experimental design and statistical models*. *Archaeometry*, **2**, 339–364.

Guyez, A., **Bonnet, S.**, **Reimann, T.**, **Carretier, S.** and **Wallinga, J.** (2023) A Novel Approach to Quantify Sediment Transfer and Storage in Rivers—Testing Feldspar Single-Grain pIRIR Analysis and Numerical Simulations. *J. Geophys. Res. Earth*, **128**, e2022JF006727. https://doi.org/10.1029/2022JF006727.

Heunks, E. and **van de Geer, P.** (2021) Landschappelijk booronderzoek Ooijpolder: een onderzoek naar de ligging en ouderdom van de restgeulen in het westelijke deel van de Ooijpolder, gemeente Berg en Dal.

Hobo, N., **Makaske, B.**, **Wallinga, J.** and **Middelkoop, H.** (2014) Reconstruction of eroded and deposited sediment volumes of the embanked River Waal, The Netherlands, for the period AD 1631-present. *Earth Surf. Process. Landf.*, **39**, 1301–1318.

Leeder, M. and **Bridges, P.** (1975) Flow separation in meander bends. *Nature*, **253**, 338–339.

Leopold, L.B. and **Wolman, M.G.** (1966) River meanders. *Bull. Geol. Soc. Am.*, **71**, 769–793.

Makaske, B. and **Weerts, H.J.T.** (2005) Muddy lateral accretion and low stream power in a sub-recent confined channel belt, Rhine-Meuse delta, central Netherlands. *Sedimentology*, **52**, 651–668.

Middelkoop, H. and **Haselen, C.O.G.v.** (1999) Twice a river: Rhine and Meuse in the Netherlands. RIZA report 99.003, ISBN 9036952239.

Mulder, J. (1989) De bodemgesteldheid van het herinrichtingsgebied 'Ooypolder'.

Murray, A.S. and **Wintle, A.G.** (2000) Luminescence dating of quartz using an improved single-aliquot regenerative-dose protocol. *Radiat. Meas.*, **32**, 57–73.

Nanson, G. (1980) Point bar and floodplain formation of the meandering Beatton River, northeastern British Columbia, Canada. *Sedimentology*, **27**, 3–29.

Nanson, G. and **Croke, J.** (1992) A genetic classification of floodplains. *Geomorphology*, **4**, 459–486.

Nicoll, T.J. and **Hickin, E.J.** (2010) Planform geometry and channel migration of confined meandering rivers on the Canadian prairies. *Geomorphology*, **116**, 37–47.

Page, K. and **Nanson, G.** (1982) Concave-bank benches and associated floodplain formation. *Earth Surf. Process. Landf.*, **7**, 529–543.

Prescott, J.R. and **Hutton, J.T.** (1994) Cosmic ray contributions to dose rates for luminescence and ESR dating: Large depths and long-term time variations. *Radiat. Meas.*, **23**, 497–500.

Preusser, F., **Degering, D.**, **Fuchs, M.**, **Hilgers, A.**, **Kadereit, A.**, **Klasen, N.** and **Spencer, J.** (2008) Luminescence dating: basics, methods and applications. *E&G Quatern. Sci. J.*, **57**, 95–149.

Quik, C. and **Wallinga, J.** (2018) Reconstructing lateral migration rates in meandering systems – A novel Bayesian approach combining optically stimulated luminescence (OSL) dating and historical maps. *Earth Surf. Dyn.*, **6**, 705–721.

Rhodes, E., **Ramsey, C.**, **Outram, Z.**, **Batt, C.**, **Willis, L.**, **Dockrill, S.** and **Bond, J.** (2003) Bayesian methods applied to the interpretation of multiple OSL dates: high precision sediment ages from Old Scatness Broch excavations. *Shetland Isles. Quatern. Int.*, **22**, 1231–1244.

Rittenour, T.M. (2008) Luminescence dating of fluvial deposits: Applications to geomorphic, palaeoseismic and archaeological research. *Boreas*, **37**, 613–635.

Rodnight, H., **Duller, G.A.T.**, **Tooth, S.** and **Wintle, A.G.** (2005) Optical dating of a scroll-bar sequence on the Klip River, South Africa, to derive the lateral migration rate of a meander bend. *Holocene*, **15**, 802–811.

Schnauder, I. and **Sukhodolov, A.N.** (2012) Flow in a tightly curving meander bend: Effects of seasonal changes in aquatic macrophyte cover. *Earth Surf. Process. Landf.*, **37**, 1142–1157.

Schwartz, J.S. and **Herricks, E.E.** (2005) Fish use of stage-specific fluvial habitats as refuge patches during a flood in a low-gradient Illinois stream. *Can. J. Fish. Aquat. Sci.*, **62**, 1540–1552.

Smedley, R.K. and **Skirrow, G.K.A.** (2020) Luminescence dating in fluvial settings: overcoming the challenge of partial bleaching. In: *Paleohydrology: Traces, Tracks and Trails of Extreme Events* (Eds Herget, J. and Fontana, A.), pp. 155–168. Springer Nature, Switzerland.

Smith, D.G., **Hubbard, S.M.**, **Leckie, D.A.** and **Fustic, M.** (2009) Counter point bar deposits: Lithofacies and reservoir significance in the meandering modern peace river and ancient McMurray formation, Alberta, Canada. *Sedimentology*, **56**, 1655–1669.

Smith, D.G., **Hubbard, S.M.**, **Lavigne, J.R.**, **Leckie, D.A.** and **Fustic, M.** (2011) Stratigraphy of counter-point-bar and eddy-accretion deposits in low-energy meander belts of the peace-athabasca delta, northeast Alberta, Canada. from river to rock record. In: *From River to Rock Record: the Preservation of Fluvial Sediments and Their Subsequent Interpretation* (Eds Davidson, S.K., Leleu, S. and North, C.P., pp. 143–152. SEPM, Special Publication.

Stouthamer, E. and **Berendsen, H.J.A.** (2001) Avulsion frequency, avulsion duration, and intervulsion period of holocene channel belts in the Rhine-Meuse delta, The Netherlands. *Nederlandse Geografische Stud.*, **71**, 105–126.

Sylvester, Z., **Durkin, P.**, **Covault, J.A.** and **Sharman, G.R.** (2019) High curvatures drive river meandering. *Geology*, **47**, e486.

Sylvester, Z., **Durkin, P.R.**, **Hubbard, S.M.** and **Mohrig, D.** (2021) Autogenic translation and counter point bar deposition in meandering rivers. *Bull. Geol. Soc. Am.*, **133**, 2439–2456.

Thijssen, J. and **Wildenberg, J.** (2005) Vondsten uit de klei. Een verkennend archeologisch onderzoek in het Circul van Ooij-gemeente Ubbergen.

Truelsen, J. and **Wallinga, J.** (2003) Zeroing of the OSL signal as a function of grain size: investigating bleaching and thermal transfer for a young fluvial sample. *Geochronometria*, **22**, 1–8.

Van den Broek, P., **van Enckevort, H.** and **Thijssen, J.** (2009) "De oeverbewoners noemen hem Vahalis". De Waal bij Nijmegen in de Romeinse tijd. In: *Jaarboek Numaga LVI*, pp. 15–31. Vereniging Numaga, Nijmegen.

Van der Heijden, P. (2016) Grens van het Romeinse rijk. In: *De limes in Gelderland* (Ed Matrijs). Uitgeverij Matrijs, Utrecht.

Verhagen, J.G.M., **Kluiving, S.J.**, **Anker, E.**, **van Leeuwen, L.** and **Prins, M.A.** (2017) Geoarchaeological prospection for Roman waterworks near the late Holocene Rhine-Waal delta bifurcation, The Netherlands. *Catena*, **149**, 460–473.

Vermeulen, B., **Hoitink, A.**, **Van Berkum, S.** and **Hidayat, H.** (2014) Sharp bends associated with deep scours in a tropical river: The river Mahakam (East Kalimantan, Indonesia). *J. Geophys. Res. Earth*, **119**, 1441–1454.

Wallinga, J. (2002) Optically stimulated luminescence dating of fluvial deposits: a review. *Boreas*, **31**, 303–322.

Wallinga, J. and **Bos, I.J.** (2010) Optical dating of fluvio-deltaic clastic lake-fill sediments – A feasibility study in the Holocene Rhine delta (western Netherlands). *Quatern. Geochronol.*, **5**, 602–610.

Wallinga, J. and **Cunningham, A.** (2014) Luminescence dating, uncertainties and age range. In: *Encyclopedia of Scientific Dating Methods* (Eds Rink, W. and Thompson, J.). Springer, Dordrecht. https://doi.org/10.1007/978-94-007-6326-5_197-1.

Wallinga, J. and **Van der Staay, J.** (1999) Sampling in waterlogged sands with a simple hand-operated corer. *Ancient TL*, **17**, 59–61.

Wallinga, J., **Hobo, N.**, **Cunningham, A.**, **Versendaal, A.**, **Makaske, B.** and **Middelkoop, H.** (2010) Sedimentation rates on embanked floodplains determined through quartz optical dating. *Quatern. Geochronol.*, **5**, 170–175.

Willems, W. (1986) Romans and Batavians. A Regional Study in the Dutch Eastern River Area, II. In: *Berichten van de Rijksdienst voor het Oudheidkundig Bodemonderzoek*, Vol. **34**. Doctoral Thesis. Leiden University, Leiden.

Willems, W. (1990) Romeins Nijmegen. Vier eeuwen stad en centrum aan de Waal.

Willemse, N. (2019) De vroege Waal bij Nijmegen. Stratigrafie, sedimentologie en genese van laatholocene rivierafzettingen tussen Nijmegen en Lent. RAAP-Rapport 3208.

Winkels, T., **Stouthamer, E.**, **Cohen, K.** and **Middelkoop, H.** (2020) Geological framework for explaining sedimentological variability underneath river dikes in the Rhine-Meuse delta, The Netherlands. *Eng. Geol.*, **73**, 106362.

Winkels, T.G., **Stouthamer, E.** and **Cohen, K.M.** (2022) Planform architecture, meander evolution and grain-size variability of a deltaic channel belt in the Rhine-Meuse Delta, The Netherlands. *Sedimentology*, **69**, 2844–2866. https://doi.org/10.1111/sed.13022.

Supporting Information

Additional information may be found in the online version of this article:

Fig. S1. Borehole logs of transect A made using LLG (Cohen, 2012).

Fig. S2. Borehole logs of transect B made using LLG (Cohen, 2012).

Fig. S3. Radial plots showing the measured D_e (equivalent dose) distributions for each OSL sample. Filled circles fall within 2σ of the mean burial dose calculated by the central age model (blue shading).

Table S1. Single aliquot regenerative dose (SAR) protocol used (following Murray & Wintle, 2000).

Table S2. Optically stimulated luminescence (OSL) sample radionuclide concentrations and organic matter contents used for calculating dose rate.

Table S3. Dose rate contributions for OSL samples.

Table S4. Migration rates between individual samples calculated using the unshared (random) errors on the estimated ages.